The Astrophysical Journal, 642:470–477, 2006 May 1

δ CETI IS NOT MONOPERIODIC: SEISMIC MODELING OF A β CEPHEI STAR FROM *MOST*[1] SPACE-BASED PHOTOMETRY

C. Aerts,[2,3] S. V. Marchenko,[4] J. M. Matthews,[5] R. Kuschnig,[5] D. B. Guenther,[6] A. F. J. Moffat,[7] S. M. Rucinski,[8] D. Sasselov,[9] G. A. H. Walker,[10] and W. W. Weiss[11]

Received 2005 November 22; accepted 2005 December 29

ABSTRACT

The β Cephei star δ Ceti was considered one of the few monoperiodic variables in its class. Despite (or perhaps because of) its apparently simple oscillation spectrum, it has been challenging and controversial to identify this star's pulsation mode and constrain its physical parameters seismically. Broadband time-resolved photometry of δ Ceti spanning 18.7 days with a duty cycle of about 65% obtained by the *Microvariability and Oscillations of Stars* (*MOST*) satellite—the first scientific observations ever obtained by *MOST*—reveals that the star is actually multiperiodic. Besides the well-known dominant frequency of $f_1 = 6.205886$ day^{-1}, we have discovered in the *MOST* data its first harmonic $2f_1$ and three other frequencies ($f_2 = 3.737, f_3 = 3.673$, and $f_4 = 0.318$ day^{-1}), all detected with a signal-to-noise ratio (S/N) > 4. In retrospect, f_2 was also present in archival spectral line-profile data but at lower S/N. We present seismic models whose modes match exactly the frequencies f_1 and f_2. Only one model falls within the common part of the error boxes of the star's observed surface gravity and effective temperature from photometry and spectroscopy. In this model, f_1 is the radial ($l = 0$) first overtone, and f_2 is the g_2 ($l = 2, m = 0$) mode. This model has a mass of $10.2 \pm 0.2\ M_\odot$ and an age of 17.9 ± 0.3 Myr, making δ Ceti an evolved β Cephei star. If f_2 and f_3 are rotationally split components of the same g_2 mode, then the star's equatorial rotation velocity is either 27.6 km s^{-1} or half this value. Given its $v \sin i$ of about 1 km s^{-1}, this implies that we are seeing δ Ceti nearly pole-on.

Subject headings: stars: early-type — stars: individual (HD 16582) — stars: oscillations — stars: variables: other

1. INTRODUCTION

Asteroseismic modeling of β Cephei pulsators offers an important window on the structure and evolution of massive evolved B stars, which are precursors to core-collapse supernovae. Significant progress has been made recently thanks to ground-based single-site photometric campaigns lasting many years and multisite synoptic campaigns lasting several months. The first method made possible the identification of six pulsation modes in HD 129929 (B3 V), leading to the first observational proof of nonrigid rotation inside a star other than the Sun (Aerts et al. 2003). The second method resulted in the identification of about 20 frequencies in the star ν Eri (B2 III; Handler et al. 2004; Aerts et al. 2004; De Ridder et al. 2004) and a second strong case for differential internal rotation (Pamyatnykh et al. 2004) in a massive B star. These successes have prompted similar studies of other β Cephei stars; e.g., θ Oph (B2 IV; Handler et al. 2005; Briquet et al. 2005) and 12 Lac (B2 III; Handler et al. 2006). Photometry from a space-based platform offers the advantages of both methods, producing a longtime series of much higher duty cycles than are possible from the ground. This paper is an indication of what is possible when such data become available for even a seemingly simple β Cephei star, which has been investigated for decades with only limited progress.

The bright star δ Ceti ($m_V = 4.07$, B2 IV) is one of the very few β Cephei stars thought to be a monoperiodic pulsator within that class (Stankov & Handler 2005 and references therein). Its variability has been investigated in a number of ground-based studies, most of which were based on only a few nights of data. A clear overview of these studies up to 1987 is not repeated here, since it can be found already in Jerzykiewicz et al. (1988), who investigated the star's behavior from multicolor photometry taken during seven consecutive nights in 1981 and one night in 1982, as well as from archival data. These authors put forward one oscillation frequency equal to 6.20587545 day^{-1} with an amplitude of $\approx$12 mmag from data assembled between 1963 and 1982. From their new data, they found night-to-night variations of the mean brightness and of the amplitude in the *uvby* filters. They attributed the amplitude variability to either a secondary short period with an amplitude below 1.6 mmag, a slow drift in the data, or both. They did not find any night-to-night phase variations.

Kubiak & Seggewiss (1990) collected two nights of simultaneous spectroscopic and photoelectric observations of the star and confirmed the phase lag between the radial velocity and light curves of 0.23 found in earlier studies.

Aerts et al. (1992) discovered large-amplitude line-profile variations in δ Ceti, from which they identified the single frequency as a radial mode with a velocity amplitude of 7.4 ± 0.1 km s^{-1}. This identification was confirmed from available multicolor photometry by Cugier et al. (1994) and Cugier & Nowak (1997).

[1] Based on data from the *MOST* satellite, a Canadian Space Agency mission, jointly operated by Dynacon Inc., the University of Toronto Institute for Aerospace Studies, and the University of British Columbia, with the assistance of the University of Vienna.

[2] Institute of Astronomy, University of Leuven, Celestijnenlaan 200 B, B-3001 Leuven, Belgium; conny@ster.kuleuven.be.

[3] Department of Astrophysics, Radboud University Nijmegen, P.O. Box 9010, 6500 GL Nijmegen, Netherlands.

[4] Department of Physics and Astronomy, Western Kentucky University, 1906 College Heights Boulevard, 11077, Bowling Green, KY 42101-1077.

[5] Department of Physics and Astronomy, University of British Columbia, 6224 Agricultural Road, Vancouver, BC V6T 1Z1, Canada.

[6] Department of Astronomy and Physics, St. Mary's University, Halifax, NS B3H 3C3, Canada.

[7] Département de Physique, Université de Montréal, C.P. 6128, Succursale Centre-Ville, Montréal, QC H3C 3J7, Canada.

[8] David Dunlap Observatory, University of Toronto, P.O. Box 360, Richmond Hill, ON L4C 4Y6, Canada.

[9] Harvard-Smithsonian Center for Astrophysics, 60 Garden Street, Cambridge, MA 02138.

[10] 1234 Hewlett Place, Victoria, BC V8S 4P7, Canada.

[11] Institut für Astronomie, Universität Wien, Türkenschanzstrasse 17, A-1180 Vienna, Austria.

Finally, Daszyńska-Daszkiewicz et al. (2005) tried to put constraints on the internal physics of the star and to identify the radial order of the mode from combined multicolor photometry and radial velocity data. They found significant differences between the data and their seismic models depending on whether they adopted OPAL or OP opacities, and they could not conclude definitely whether δ Ceti was pulsating in the radial fundamental or first overtone mode. Neither model scenario could be made to agree with the observations.

New space-based observations of δ Ceti by the *MOST* satellite have now provided key clues to understanding this star. The first ground-based observations of δ Ceti were obtained over a century ago, and over the course of the last three to four decades there has been a prolonged debate about its amplitude modulation, possible multiperiodicity, and period changes. In that time, a grand total of about 30 cycles of its dominant pulsation mode have been monitored. In less than 3 weeks, *MOST* was able to thoroughly sample over 70 cycles.

2. OBSERVATIONS AND DATA REDUCTION

The *MOST* satellite (Walker et al. 2003), housing a 15 cm Rumak-Maksutov optical telescope feeding a charge-coupled device (CCD) photometer, was launched in 2003 June. Its primary mission is ultraprecise rapid photometry for asteroseismology. *MOST* was designed to monitor stars at a rate as high as 10 times per minute with a single-point precision of about 1–2 mmag. For stars within the satellite's continuous viewing zone (CVZ)—in a declination range $-18^\circ \leq \delta \leq +36^\circ$—data can be collected nearly without interruption for up to 8 weeks. The combination of single-point precision and longtime coverage with high duty cycle leads to sensitivity to rapid oscillations in Fourier space as low as about 1 μmag = 1 parts per million (ppm). An example of the photometric precision can be seen in Matthews et al. (2004).

During the early stages of the mission when *MOST* was being checked out for routine scientific operations, the *MOST* Team decided to use δ Ceti (conveniently located in the CVZ) as its first test target, for what was designated Commissioning Science. At the time of the δ Ceti observations—the first scientific data collected by *MOST*—the spacecraft pointing had not yet been optimized, debugging of onboard software led to computer crashes that introduced gaps into the time series, and the downlink to Earth did not yet permit the nominal science data sampling rate. Hence, the photometric precision and duty cycle were far from what *MOST* was capable of achieving once commissioning was complete. However, at the time, this light curve represented the best combination of precision, duration, and duty cycle ever obtained for any astronomical object other than the Sun.

MOST monitored δ Ceti for 18.68 days during 2003 October 8–27, with 10 s exposures at a sampling interval of 120 s. The data were obtained through a broadband filter designed expressly for the *MOST* instrument, with a bandpass of about 350–700 nm and a throughput approximately 3 times that of a Johnson V filter. The data were reduced independently by two of the authors (S. M. and R. K.), yielding similar results. We present here the S. M. reduction, described below.

The principal observing mode for *MOST* is known as Fabry imaging, in which the light from a bright star illuminates a Fabry microlens, which projects an image of the telescope pupil onto the CCD (see Walker et al. [2003] and their Fig. 10). The star is centered in a field stop $1'$ in diameter, and the doughnut-shaped pupil image covers about 1300 pixels in a square CCD subraster of 58 pixels on a side. Seven adjacent Fabry microlenses sample the surrounding sky background. (One neighboring lens is not used because its reading is contaminated by light from the star as pixels are transferred under the target star beam during readout.)

Data are returned to Earth in two formats, or science data streams, known as SDS1 and SDS2. The former are processed on board so that only a small set of integrated numbers is sent to Earth; the latter consist of resolved Fabry images, which can be fully reduced on the ground. Because of the limitations of the commissioning performance, the quality of the SDS1 data (numbering about 10,000) was severely compromised and is not used for this reduction. The Fabry images of the δ Ceti SDS2 data were binned 2×2 to form a 29×29 pixel image. For each image, all the available estimates of biases were iteratively checked for significant outliers and, using appropriate weights, combined to provide an average for a given image.

Most of the data reduction effort is made to correct for the changing background, primarily due to orbital modulation of scattered earthshine. Detailed aspects of this stray light are described by Reegen et al. (2006). Readings from the seven adjacent Fabry microlenses (after 3 σ clipping of outliers) were used to derive unweighted averages of the background. The primary target Fabry field also contains about 350 pixels with only background that were used to calculate a third background average. This last estimate of the background turned out to give the best removal of stray light artifacts, and it alone was used for the current reduction.

Since δ Ceti was observed during satellite commissioning, and the pointing accuracy was still far from optimal, the pointing errors (with $\sigma_{X,Y} \sim 1$ pixel) were tracked for each exposure, based on the Attitude Control System telemetry. The pointing errors (and other possible inhomogeneities in the optics) were also estimated directly from the images themselves by comparing the average fluxes in the four image quadrants. Large deviations from quadrant to quadrant were flagged and could lead to rejection of an image.

After bias and background subtraction, each Fabry target image was assigned a quality rank. This was calculated by adding "penalties" and rejecting all images with a penalty count exceeding 3. Any large deviation (>3.5 σ above average) in the X or Y pointing of the satellite (updated once per second), added 1 to the penalty count. A similarly large deviation of the $(X^2 + Y^2)$ pointing vector, as well as an excessive number of >3.5 σ shifts from the average position in a 10 s exposure (more than three such deviations in a set of 10 successive readings), added 1.5 each to the penalty. Any large systematic shift (>5 pixels, either in X or Y) of the 10 s average from the global average position from the entire run resulted in immediate rejection of the image. The rest of the quality ranking was based on dividing each Fabry image into four quadrants and assessing the uniformity across these quadrants. An iterative calculation of the percentage of outlying pixels in each quadrant (usually due to cosmic-ray strikes or hot pixels in the CCD) sets the next component of the rank. If the number of rejected pixels exceeded 5% or 10%, the penalty was increased by 1 or 2, respectively. An image was rejected if any single quadrant contained more than 50% of the total number of faulty pixels (even if that number was below 10%), or any combination of two quadrants was responsible for 75% of the bad pixels.

The preselected pixels in each image that passed the quality control were added to produce an instrumental flux value. The instrument telemetry also includes the CCD focal plane temperature, which was not completely regulated during the commissioning observations. Correlations between CCD temperature and the image fluxes were corrected. The final stage of the reduction was high-pass filtering and 3 σ clipping of the data to remove any rapid

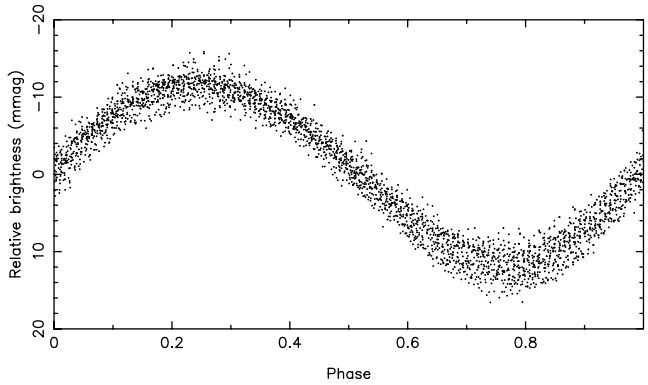

FIG. 1.—Phase diagram of the *MOST* data of δ Ceti folded at the known dominant pulsation period of 0.161138 days.

changes in stray light that survived the earlier quality tests. For the period range of relevance for δ Ceti, this is not expected to remove any intrinsic stellar signal. As a reality check, we always compared the corrected fluxes to the original raw estimates. Any large deviations ($\delta m \geq 0.005$ mag) were reexamined to avoid the danger of spurious overcorrection.

The duty cycle of the original SDS1 + SDS2 photometry was about 65%, with a stretch of 11 days reaching about 95%. The exclusion of the SDS1 data, and the data rejection above, reduces the total number of data points from 3267 to 2949. The absolute duty cycle of this filtered light curve is only 22%, but it should be noted the reduction in duty cycle is primarily in each orbital cycle of 101.4 minutes, with no regular daily gaps as in ground-based photometry. The overall sampling of the δ Ceti light curve still approaches a duty cycle of 65%.

The total standard deviation of the 2949 data point set is 8.47 mmag, which is dominated by the intrinsic pulsational variability of the star. The phase diagram of the data, folded at the known dominant pulsation period, is presented in Figure 1. This plot, and the light-curve segments shown in Figure 6, illustrate the thorough coverage and quality of the *MOST* photometry of δ Ceti.

3. DATA ANALYSIS

3.1. *Discovery of the Multiperiodicity of δ Ceti*

We computed the Scargle Fourier periodogram (Scargle 1982) of the data (Fig. 2*b*) with a sampling of 10^{-6} day^{-1} and found the expected dominant peak at $f_1 = 6.20589(8)$ day^{-1} (=71.827 μHz); $P = 0.16114$ $d = 3.867$ hr. The error estimate of 8×10^{-5} day^{-1} was computed as $\sigma_f = \sqrt{6}\,\sigma_{\rm std}/\pi\sqrt{N}\,A\,\Delta T$ (Montgomery & O'Donohue & 1999), with N as the number of measurements, A as the amplitude, ΔT as the total time span, and $\sigma_{\rm std}$ as the standard deviation of the final residuals. This value of f_1 is identical to within the errors, to the value reported by Jerzykiewicz et al. (1988). We then compared the periodogram to the spectral window function (Fig. 2*a*), which was computed from a sinusoid of the same frequency and amplitude as peak f_1 sampled at the same times as the real-time series.

A least-squares harmonic fit to the data, fixing the value of f_1 above, gives an amplitude for that peak of 11.62(3) mmag and reveals the presence of the first harmonic $2f_1$ with an amplitude of 0.72(3) mmag and a S/N of about 7.5 σ. While harmonics of principal oscillation frequencies have been found in other β Cephei stars (e.g., Heynderickx et al. 1994), one was never before detected in δ Ceti. This is not surprising, given its amplitude is only 6% of that of f_1.

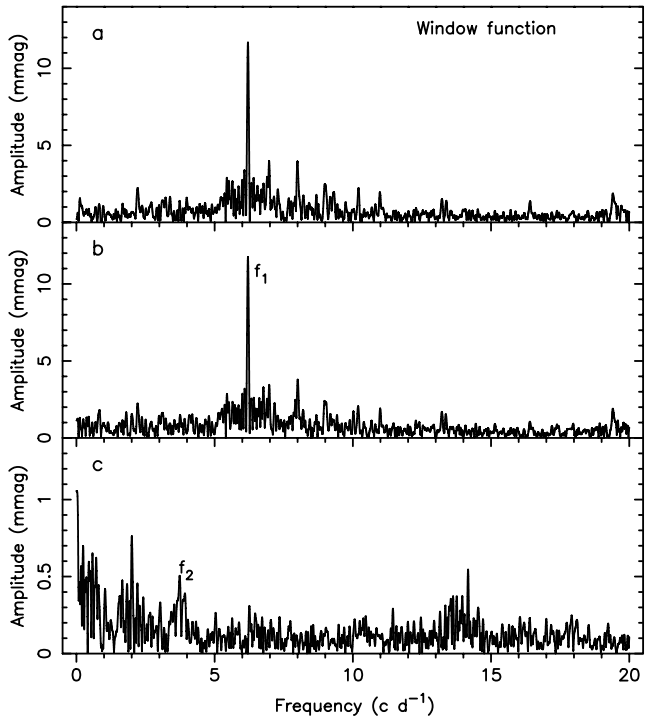

FIG. 2.—Periodograms of the *MOST* photometry of δ Ceti. (*a*) Window function shifted and scaled to the main peak. (*b*) Periodogram of the data. (*c*) Periodogram after prewhitening with f_1 and $2f_1$.

Subtracting f_1 and $2f_1$ from the data results in the periodogram shown in Figure 2*c*. The overall variance of the time series has been reduced by 96.6%, so the residuals have a standard deviation of only $\sigma = 1.56$ mmag. Four peaks are immediately obvious in Figure 2*c*: 0.02, 2.00, 3.73, and 14.20 day^{-1}. The last corresponds to the known orbital frequency of the *MOST* satellite and is an observed artifact in later *MOST* data, due to the modulation of scattered earthshine in the *MOST* focal plane with the orbital period. The 2.00 day^{-1} frequency is also almost certainly an artifact. It is due to a modulation of the stray light from the Earth as *MOST*'s Sun-synchronous dusk-dawn orbit takes it over similar features of the Earth's albedo on a daily cycle. In this case, it may be due to the maxima in the Earth's albedo near both poles, not long after the autumnal equinox.

The low-frequency peak near 0.02 day^{-1} is consistent with a long-term trend in the data, discussed below. The remaining peak, labeled f_2 in Figure 2*c*, cannot be ascribed to any known instrumental artifact and is almost certainly intrinsic to δ Ceti.

3.2. *Long-Term Variability*

In its Fabry imaging mode, *MOST* is a nondifferential experiment, with no comparison star observed in a comparable fashion in the field. However, experience with 2 yr of *MOST* data has shown that the instrument is remarkably stable. Because of the previous observation by Jerzykiewicz et al. (1988) of a monotonic amplitude change over seven consecutive nights, and the presence of a low-frequency peak in Figure 2*c*, we searched for evidence of such amplitude changes before proceeding with frequency analysis of the *MOST* photometry.

We divided the time series into subsets. Each subset was longer than the dominant period of 0.17 days but shorter than 0.5 days so as to mimic the previous ground-based data. Each subset used had at least 50 data points and no large gaps. We produced 25 such subsets and fitted them with f_1 and $2f_1$, allowing the amplitudes and phases to be free parameters. The resulting

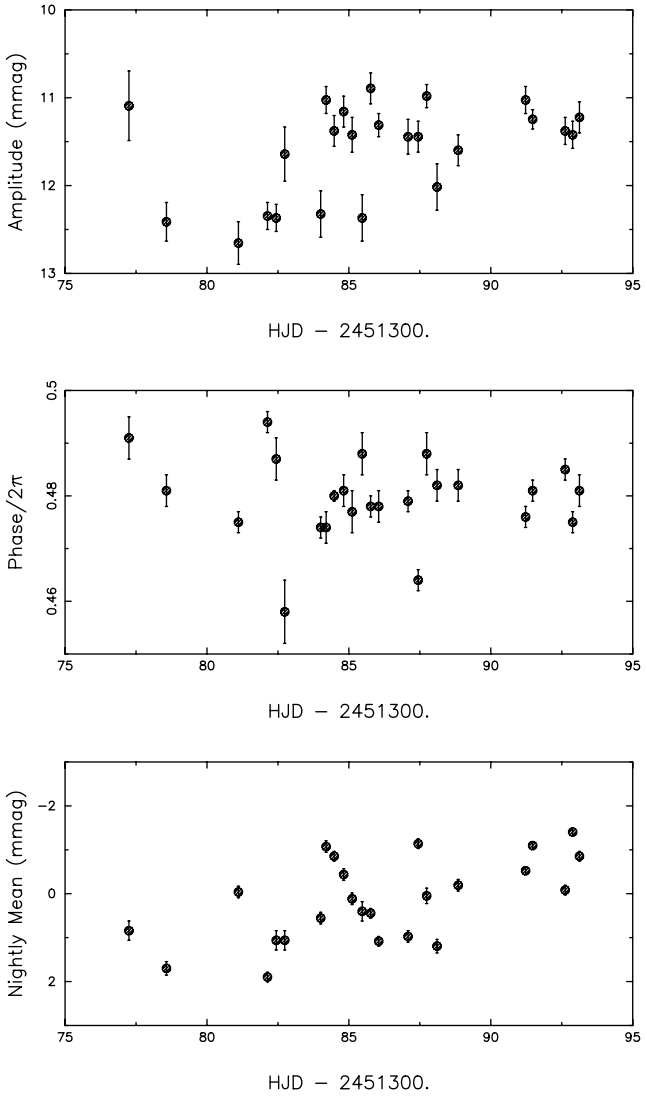

FIG. 3.—Amplitude of f_1, phase of f_1, and mean with respect to the overall mean, for 25 data strings observed by *MOST*.

amplitudes, phases, and "nightly" means of f_1 are plotted in Figure 3.

All three quantities vary beyond the error bars of the individual points, but in a complicated fashion. However, the total ranges of variability are small: about 15% in amplitude, 4% in phase, and about 0.4% in mean brightness. The mean brightness does show the clearest evidence for a trend, which turns out to be responsible for the peak near 0.02 day^{-1} ($P \sim 50$ days).

We then fitted the data residuals from § 3.1 (f_1 and $2f_1$ prewhitened) with a linear trend as shown in Figure 4. The linear fit corresponds to a brightness increase of 0.154 mmag day^{-1} = 0.0064 mmag hr^{-1}. This is more than 2 orders of magnitude smaller than the trend of about 1 mmag hr^{-1} reported by Jerzykiewicz et al. (1988) in their Strömgren photometry of δ Ceti.

We cannot confirm whether the trend seen by *MOST* is stellar or instrumental (see discussion in § 5), but we nonetheless remove it from the data for subsequent analysis. The detrended residuals have a standard deviation of 1.37 mmag, 0.19 mmag smaller than before.

3.3. *Additional Oscillation Frequencies in δ Ceti*

Removing the trend from the data presented in Figure 4 produced the periodogram shown in Figure 5*a*. Not surprisingly,

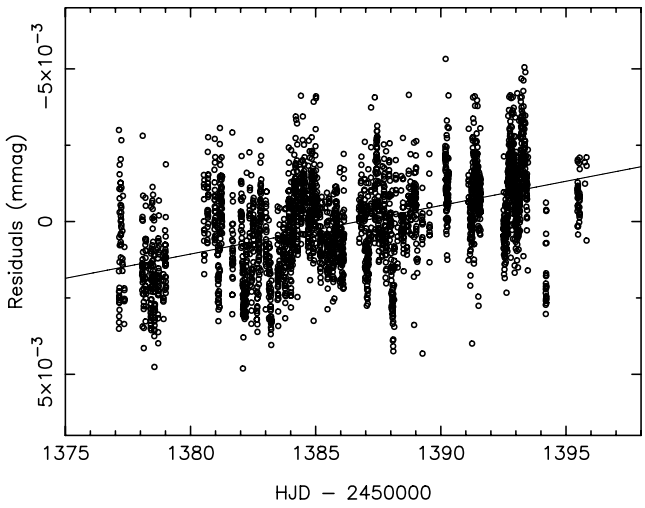

FIG. 4.—Brightness increase of δ Ceti in the residuals after prewhitening the dominant frequency f_1 and its harmonic from the *MOST* light curve.

the peak at 0.02 day^{-1} vanished. Perhaps surprisingly, the peak at 14.2 day^{-1} also disappeared. It turned out not to be due primarily to modulated stray earthshine but to the long-term trend sampled with gaps in the data at the orbital frequency (due to outages during the spacecraft commissioning phase).

The peak at 2.003 day^{-1} does remain, consistent with a genuine stray light artifact, although its amplitude has been reduced by more than half, so the trend contributed to it as well.

The frequency $f_2 = 3.737(2)$ day^{-1} persists as well, and its amplitude of 0.53(3) mmag—significant at the 5.6 σ level—is almost unchanged from the original data before the trend was removed. We note that this frequency and the dominant frequency

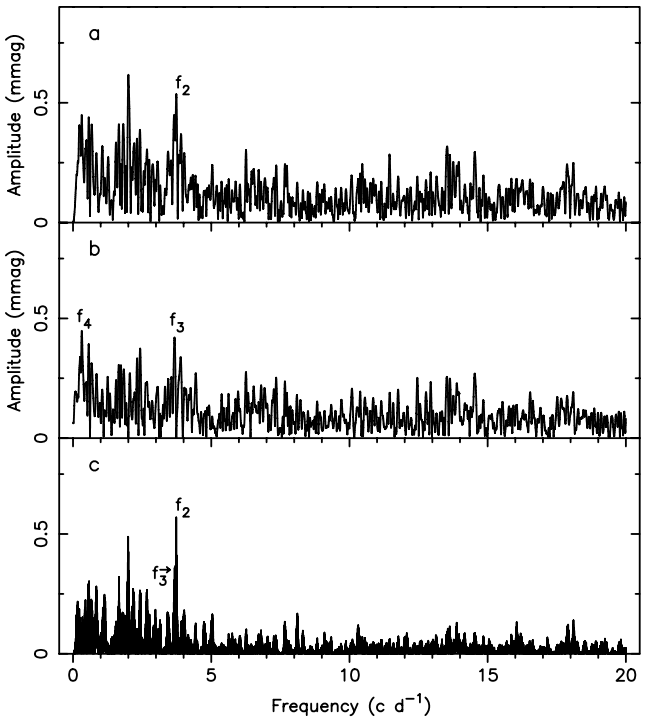

FIG. 5.—Periodograms of δ Ceti. (*a*) After prewhitening with f_1 and $2f_1$ and detrending according to Fig. 4. (*b*) After subsequent prewhitening with f_2 and 2.003 day^{-1}. (*c*) Product of normalized amplitude spectra of the *MOST* and *Hipparcos* photometry and the first velocity moment $\langle v \rangle$ taken from Aerts et al. (1992).

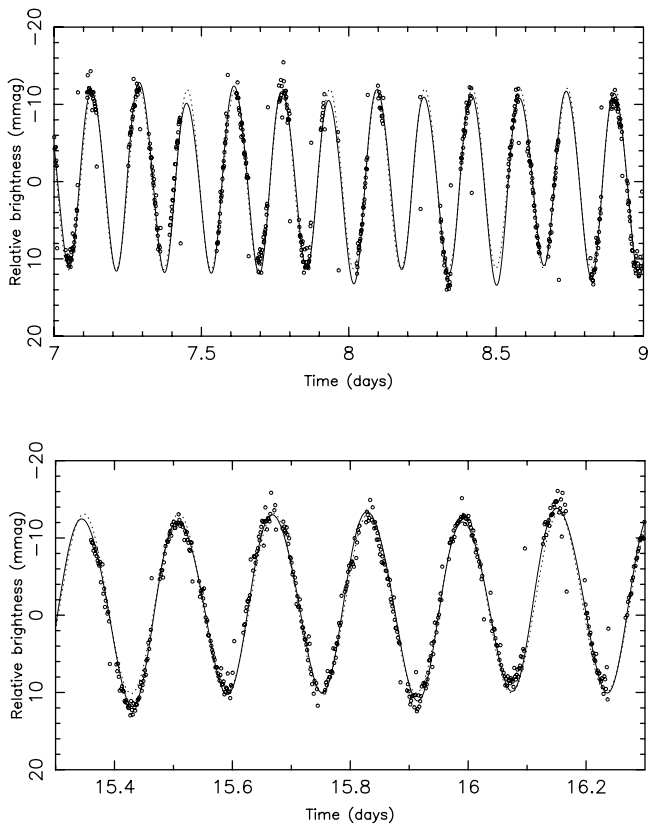

FIG. 6.—Comparison between the *MOST* data, and (1) the final fit given in eq. (1) (*solid lines*) and (2) a fit including only the dominant frequency and the trend (*dotted lines*) for a few selected segments.

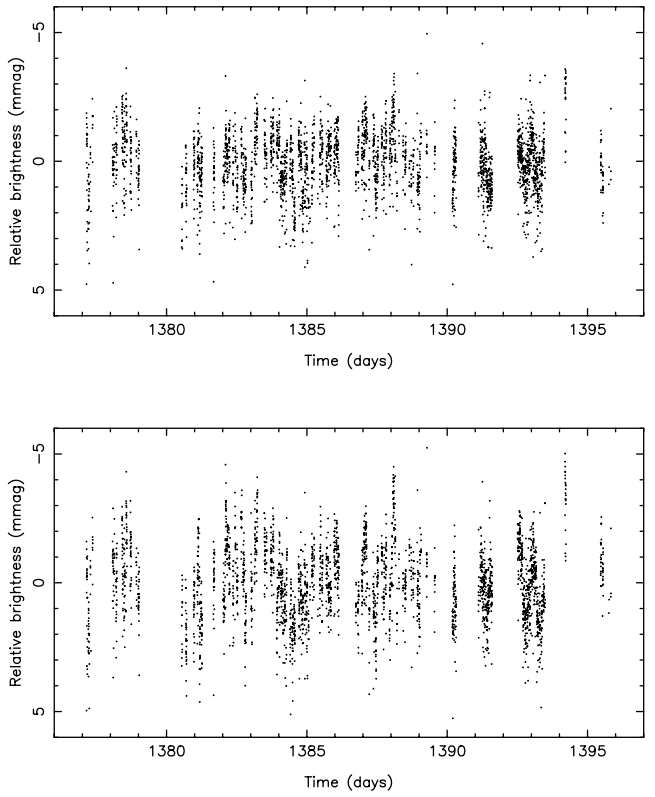

FIG. 7.—Residuals of the entire *MOST* data set after prewhitening by the final fit given in eq. (1) (*top*) and by only the dominant frequency f_1 and the linear trend in the data (*bottom*). The standard deviations of these residuals are 1.18 and 1.47 mmag, respectively.

f_1 have a beat period $1/(f_1 - f_2) = 0.405$ days $\sim$9.7 hr, which is well sampled by several continuous stretches in the *MOST* time series but not by the nightly stretches in the ground-based data of Jerzykiewicz et al. (1988).

Prewhitening the *MOST* residuals by frequency f_2 and the artifact at 2.003 day^{-1} reduces the standard deviation by 0.12–1.25 mmag. From these residuals, we obtain the periodogram plotted in Figure 5*b*. This contains two peaks with significance greater than 4 σ, namely, $f_3 = 3.673(2)$ and $f_4 = 0.318(2)$ day^{-1}, with amplitudes of 0.39(4) mmag (4.0 σ) and 0.43(4) mmag (4.5 σ), respectively.

Prewhitening the data by these two additional frequencies reduces the overall σ by only 0.07 mmag. A plot of the final residuals is given in Figure 7. Their periodogram shows several peaks with amplitudes below 0.4 mmag that may help account for the complex amplitude and phase behavior seen in Figure 3. These include a peak at 3.909(5) day^{-1} at the 3.5 σ level and one at 3.805(6) day^{-1} at the 2.8 σ level.

3.4. *Reexamination of Archival Data*

In light of this frequency analysis of the *MOST* data, we reanalyzed two high-precision archival data sets of δ Ceti:

1. the *Hipparcos* light curve (Perryman et al. 1997), consisting of 72 data points covering 1096 days with a quasi-equidistant spacing of about 15 days; and
2. the 60 moment variations derived from single-site high-resolution line-profile observations by Aerts et al. (1992), spanning 7 days.

Neither of these data sets showed any significant long-term trends. After prewhitening both independent data sets with frequency f_1, we searched for evidence of f_2 in the residuals. There was no sign of signal at f_2 in the *Hipparcos* photometry, which is not surprising given its low amplitude in the *MOST* data and the poor sampling of the *Hipparcos* data for this relatively short period. However, in a periodogram of the first velocity moment $\langle v \rangle$ computed by Aerts et al. (1992) from their line-profile data, a peak shows up near f_2, with an amplitude of 0.27 ± 0.09 km s^{-1}, corresponding to a significance of only 3 σ. Despite the low significance, and because of its presence in the *MOST* data, we conducted a second investigation of f_2 in the archival data.

The dominant frequency f_1 is present in the *Hipparcos* data with an amplitude comparable to that seen in the *MOST* data, despite the use of different custom filters for these observations. So we prewhitened the *Hipparcos* and *MOST* (detrended) light curves and the $\langle v \rangle$ moment data by f_1 and $2f_1$, and then normalized the resulting Scargle periodograms to the highest peak in each. We then multiplied these normalized periodograms together, with the logic that if f_2 (or any other common frequency) were present in more than one of the data sets, it would show up with improved S/N over the *MOST* data alone. If f_2 were absent in the other sets, it would reduce the S/N over *MOST* alone. In this exercise, all three data sets were given equal weight.

The outcome is shown in Figure 5*c*. Two peaks are immediately obvious to the eye: at f_2 and 2.00 day^{-1}. The latter has been reduced in significance, consistent with it being an artifact in the *MOST* data alone, while f_2 now has a significantly higher S/N of 8.6. Closer examination (and prewhitening) reveals the presence of a third peak at f_3 at the 4.6 σ level, higher than in the *MOST* data alone. The frequency f_4 is not evident in the combined normalized periodogram.

TABLE 1
FINAL LIGHT-CURVE SOLUTION OF δ CETI

f_j (day^{-1})	f_j (μHz)	c_j (mmag)	ϕ_j	S/N
f_1 = 6.20589(8)	71.8274(9)	11.62(3)	0.4958(4)	121.4
$2f_1$	$2f_1$	0.72(3)	0.619(7)	7.5
2.003(1)	23.18(1)	0.65(3)	0.292(7)	6.8
f_2 = 3.737(2)	43.25(2)	0.53(3)	0.454(9)	5.5
f_3 = 3.673(2)	42.51(2)	0.39(4)	0.82(1)	4.0
f_4 = 0.318(2)	3.68(2)	0.43(4)	0.55(2)	4.5

NOTES.—According to the eight terms given in eq. (1). The reference epoch for the phases ϕ_j is the time of the first measurement (HJD 2,451,377.140428). Parameters: a = 922.89(5) mmag; $b = -0.154(5)$ mmag day^{-1}.

These results lend circumstantial support to the presence of the frequencies f_2 and f_3 in one or both of the *Hipparcos* and line-profile data sets, with the a posteriori knowledge from the *MOST* photometry.

3.5. *Solution to the MOST Light Curve*

The final fit that we applied to the *MOST* light curve is as follows:

$$y_i = a + bt_i + \sum_{j=1}^{6} c_j \sin\left[2\pi\left(f_j t_i + \phi_j\right)\right], \qquad (1)$$

with the parameters provided in Table 1. We have retained only frequencies with amplitudes of significance $\geq$4.0 σ, following the acceptance criterion proposed by Breger et al. (1993) and Kuschnig et al. (1997).

Two segments of the light curve comparing this solution to the data are shown in Figure 6. The solid line corresponds to equation (1), while the dotted line is a solution including only the linear trend and the dominant frequency f_1. The residuals for the two solutions are shown in Figure 7, at a magnified vertical scale. In particular, the full solution does a much better job near the well-populated minima and maxima of the light curve and leads to smaller residuals.

4. SEISMIC INTERPRETATION

4.1. *Fitting f_1 and f_2*

To compare the oscillation frequencies we have detected in δ Ceti with those predicted by pulsational models of B-type stars, we explored the database described by Ausseloos et al. (2004). This database contains evolutionary models from the zero-age main sequence to the turnoff with masses ranging from 7 to 13 $M_\odot$ (in steps of 0.1 $M_\odot$), X fixed at 0.70, Z ranging from 0.012 to 0.030 (in steps of 0.002), and three choices for the core overshoot parameter ($\alpha_{ov} = 0.0$, 0.1, or 0.2). For a description of the input physics of these models, and the computation of their oscillation frequencies, we refer to Ausseloos et al. (2004).

Since analyses of the line-profile variations and earlier multicolor photometry indicate that the dominant pulsation frequency f_1 corresponds to a radial mode (Aerts et al. 1992; Cugier et al. 1994), we have restricted our search of the model grid to those models with radial modes that coincide with f_1. We have further constrained the search by forcing f_2 to correspond to zonal modes of $l_2 = 0$, 1, or 2, using the fitting algorithms of Ausseloos (2005). Modes with $l \geq 3$ are unlikely to be observed in integrated photometry due to cancellation effects across the stellar disk.

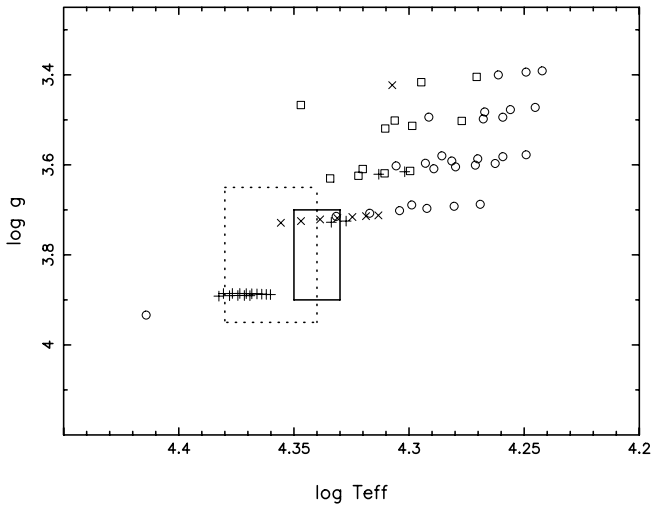

FIG. 8.—Position of stellar models in the ($\log T_{\rm eff}$, $\log g$) diagram whose zonal modes fit f_1 and f_2 simultaneously. The symbol convention is as follows: f_1 radial first overtone and f_2 an $l = 1$, $m = 0$ g mode (*circles*); f_1 radial second overtone and f_2 an $l = 1$, $m = 0g$ mode (*squares*); f_1 radial fundamental and f_2 an $l = 2$, $m = 0g$ mode (*plus signs*); and f_1 radial first overtone and f_2 an $l = 2$, $m = 0g$ mode (*crosses*). The photometric (*solid lines*) and spectroscopic (*dotted lines*) observational error boxes of δ Ceti are also indicated.

The assumption of nonzonal modes ($m \neq 0$) is considered safe since δ Ceti has a low projected rotational velocity ($v \sin i \sim 1$ km s^{-1}; Aerts et al. 1992), so even a nonzero m-component of mode f_2 should lie close to the central component of the multiplet. (See our discussion in § 4.2 about the inferred rotational velocity of δ Ceti and the validity of this assumption.)

There are no models in the database that are consistent with both f_1 and f_2 being radial ($l = 0$) modes. We found 66 models that satisfy the criteria that f_1 is a radial mode and f_2 is an $l = 1$ or 2 mode: 40 models for the former and 26 for the latter. All the models fitting f_1 and f_2 simultaneously are indicated in the theoretical ($\log T_{\rm eff}$, $\log g$) diagram shown in Figure 8.

We also have independent empirical constraints on the position of δ Ceti in Figure 8. We plot the star's empirical error box derived from photometric colors averaged over the dominant pulsation cycle in three different systems (Walraven, Geneva, and Strömgren) as determined by Heynderickx et al. (1994). We also show the spectroscopic error box recently derived by Morel et al. (2006), based on high-resolution echelle spectra covering the whole pulsation cycle. We prefer this over previous estimates relying on a single spectrum during the cycle (e.g., Gies & Lambert 1992). We put more weight on the photometric error box due to its smaller extent and the fact that it is based on three different photometric systems.

It can be seen in Figure 8 that the majority of the models matching both f_1 and f_2 are too evolved (i.e., have too low gravities) for the photometric and spectroscopic error boxes. In fact, only five models fall within the photometric box; their physical characteristics are listed in Table 2. The nonradial mode corresponding to f_2 is the g_2 mode for all of these models. All these models require some amount of core overshooting.

Which of these models is most likely to be excited? We checked the excitation rates with the nonadiabatic code MAD (Dupret 2001) and found that the radial first overtone of model 1 in Table 2 (Fig. 8, *circles*) is expected to be stable due to its low metallicity ($Z = 0.012$). All eight modes of the other four models were found to be excited.

TABLE 2
PHYSICAL PARAMETERS OF THE STELLAR MODELS WITHIN THE PHOTOMETRIC ERROR BOX OF δ CETI SHOWN IN FIG. 8

Symbol	log $L/L_\odot$	log $T_{\rm eff}$	log g	M ($M_\odot$)	R ($R_\odot$)	X_c	X	Z	$\alpha_{\rm ov}$	Age (10^6 yr)
1 (*circles*)	3.977	4.332	3.714	9.43	7.06	0.088	0.70	0.012	0.0	19.7
2 (*plus signs*)	4.014	4.334	3.727	10.36	7.29	0.252	0.70	0.028	0.1	16.9
3 (*crosses*)	4.064	4.347	3.725	10.23	7.27	0.249	0.70	0.020	0.2	17.9
4 (*crosses*)	4.026	4.339	3.721	10.04	7.23	0.255	0.70	0.022	0.2	18.6
5 (*crosses*)	3.992	4.331	3.718	9.88	7.20	0.260	0.70	0.024	0.2	19.3

NOTE.—The core overshoot parameter is expressed in units of the local pressure scale height.

The high metallicity ($Z = 0.028$) of model 2 (where f_1 is the radial fundamental mode; Fig. 8, *plus signs*) may also rule it out, since evidence points to δ Ceti having a lower value of Z than this. Niemczura & Daszyńska-Daszkiewicz (2005) recently derived $[m/{\rm H}] = -0.24 \pm 0.09$ from UV iron transitions measured by the *International Ultraviolet Explorer*. Morel et al. (2006) have derived the abundances of several important Z-determining elements from optical echelle spectra and found them to be only slightly less on average than solar values from Grevesse & Sauval (1998); $Z = 0.02$.

We conclude therefore that the dominant mode of δ Ceti is the radial first overtone. Cugier et al. (1994) and Cugier & Nowak (1997) reached the same conclusion previously, but Daszyńska-Daszkiewicz et al. (2005) recently cast doubt on this identification, citing an excitation problem. Our nonadiabatic analysis shows that this mode is unstable for our models 3, 4, and 5. Of these options, we prefer model 3 because (1) it is situated in the overlapping region of the photometric and spectroscopic error boxes, and (2) it has a metallicity ($Z = 0.020$) consistent with values derived from high-quality spectra (whereas the other two models appear to be too metal-rich). The frequency f_2 in this model is the $g_2 l = 2$ mode.

4.2. *Multiplet Structure in the δ Ceti Eigenspectrum?*

What of frequency $f_3 = 3.673$ day^{-1}? We note that it is separated from f_2 by $\Delta f = 0.064$ day^{-1}. If f_3 is part of a rotationally split multiplet, then there should be another sidelobe frequency at $f_2 + \Delta f = 3.801$ day^{-1}. Note that we did find a peak in the *MOST* data at a frequency of 3.805 day^{-1} but with a significance of only 2.8 σ.

If f_2 and f_3 are consecutive m-values ($\Delta m = 1$) of the same $l = 2$ quintuplet, and we adopt the Ledoux coefficient $\beta_{-2,2} = 0.85$ and radius of model 3, we obtain a rotational frequency of 0.075 day^{-1} and an equatorial rotation velocity of 27.6 km s^{-1}. If they are separated by $\Delta m = 2$, then we derive half these values.

If we combine these values with the well-measured value of $v \sin i = 1 \pm 1$ km s^{-1} (Aerts et al. 1992), the inclination angle of δ Ceti may be as small as $i = 2^\circ$ (and cannot be larger than $i = 8^\circ$). Hence we must be observing the star nearly pole-on. This conclusion is independent of the choice of models in Table 2.

The pole of a star corresponds to an angle of complete cancellation for an $l = 2$ sectoral and tesseral mode (Chadid et al. 2001, their Table A.1). It is therefore most likely that f_2 corresponds to the central peak of the quintuplet, as assumed in the modeling. Even if it were the outermost component of the quintuplet, the central peak would differ only by $\simeq$0.13 day^{-1} from f_2. Such a frequency shift is not large enough to affect our model identifications, which assumed a low rotation rate and hence closely spaced multiplet structure.

We also called attention in § 3.3 to another frequency, at 3.909 day^{-1}, with a significance of 3.5 σ. This frequency would not fit into an equidistant quintuplet structure that includes f_2 and f_3. We do note that model 3 has a g_3 $l = 3$ mode predicted to be excited whose frequency is close to 3.909 day^{-1}.

Finally, we have no obvious explanation for frequency $f_4 = 0.318$ day^{-1}, but we do point out that $f_4 \simeq 5(f_2 - f_3) \simeq 3(3.909 - 3.805)$ day^{-1}, within the errors. Perhaps it is related to beating between modes.

5. SUMMARY

MOST photometry of the β Cephei star δ Ceti—until now regarded as a prototypical example of a monoperiodic radial oscillator within the class—reveals the presence of at least two additional oscillations consistent with nonradial modes, as well as the first harmonic of the dominant radial mode. We have compared the new frequency spectrum with pulsation models constrained by stellar parameters based on photometric colors and spectroscopic analysis. We conclude that the dominant mode in δ Ceti is due to the radial first overtone and that the next strongest mode is the g_2 $l = 2$ mode. We investigated multiplet structure associated with the latter mode to constrain the rotational velocity of the star and showed that δ Ceti is seen nearly pole-on.

We also find a shallow linear brightness increase in the star, at a rate of about 0.0064 mmag hr^{-1}. Jerzykiewicz et al. (1988) also found a drift in their *ubvy* photometry of δ Ceti, but at a rate of about 1 mmag hr^{-1}. If both trends were truly intrinsic to the star, then the rate of brightness change would be strongly variable as a function of epoch. Such variations would not be surprising for an evolved star like δ Ceti undergoing small instabilities on its way to the end of the central hydrogen-burning phase. However, it is still possible that the trend seen by Jerzykiewicz et al. (1988) was an uncorrected effect of extinction in the Earth's atmosphere. *MOST* does not suffer such extinction effects in orbit, but as a nondifferential experiment, it is impossible to exclude an instrumental origin for the gradual trend it measured.

We note that Jerzykiewicz et al. (1988) also observed amplitude modulation in their night-to-night photometry, which they suggested might be due to a second short-period variation with an amplitude below 1.6 mmag. The detection by *MOST* of frequency f_2, with an amplitude of about 0.5 mmag, is consistent with that explanation.

The best model fit indicates that δ Ceti has a mass of $M = 10.2 \pm 0.2$ $M_\odot$, an age of 17.9 ± 0.3 Myr, and core overshooting ($\alpha_{\rm ov} = 0.20 \pm 0.05$). It is only the third β Cephei star for which the core overshooting parameter could be determined, along with HD 129929 ($\alpha_{\rm ov} = 0.10 \pm 0.05$; Aerts et al. 2003) and ν Eridani ($\alpha_{\rm ov} < 0.13$; Pamyatnykh et al. 2004). The determination of the core overshooting parameter results in an accurate seismic mass estimate, which is for all three stars an

improvement by an order of magnitude over previous photometric or spectroscopic mass estimates.

These results illustrate the power of nearly continuous ultraprecise photometry in understanding the structure and evolution of β Cephei stars. We can anticipate additional results from the space-based observatories the *Wide-Field Infrared Explorer* (H. Brüntt & D. L. Buzasi 2006, in preparation), *MOST*, the *Convection, Rotation, and Planetary Transits*, and *Kepler* in the coming years.

C. A. is indebted to Peter De Cat, Richard Scuflaire, Marc-Antoine Dupret, and Mario Ausseloos for the use of their software. C. A. is supported by the Research Council of the K. U. Leuven under grant GOA/2003/04. S. M. acknowledges financial support from the Kentucky Space Grant Consortium. J. M. M., D. B. G., A. F. J. M., S. R., and G. A. H. W. acknowledge funding from the Natural Sciences and Engineering Research Council (NSERC) of Canada. R. K.'s work is supported by the Canadian Space Agency.

REFERENCES

Aerts, C., De Pauw, M., & Waelkens, C. 1992, A&A, 266, 294
Aerts, C., et al. 2003, Science, 300, 1926
———. 2004, MNRAS, 347, 463
Ausseloos, M. 2005, Ph.D. thesis, Katholieke Univ. (Leuven)
Ausseloos, M., Scuflaire, R., Thoul, A., & Aerts, C. 2004, MNRAS, 355, 352
Breger, M., et al. 1993, A&A, 271, 482
Briquet, M., Lefever, K., Uytterhoeven, K., & Aerts, C. 2005, MNRAS, 362, 619
Chadid, M., De Ridder, J., Aerts, C., & Mathias, P. 2001, A&A, 375, 113
Cugier, H., Dziembowski, W. A., & Pamyatnykh, A. A. 1994, A&A, 291, 143
Cugier, H., & Nowak, D. 1997, A&A, 326, 620
Daszyńska-Daszkiewicz, J., Dziembowski, W. A., & Pamyatnykh, A. A. 2005, A&A, 441, 641
De Ridder, J., et al. 2004, MNRAS, 351, 324
Dupret, M.-A. 2001, A&A, 366, 166
Gies, D. R., & Lambert, D. L. 1992, ApJ, 387, 673
Grevesse, N., & Sauval, A. J. 1998, Space Sci. Rev., 85, 161
Handler, G., Shobbrook, R. R., & Mokgwetsi, T. 2005, MNRAS, 362, 612
Handler, G., et al. 2004, MNRAS, 347, 454
———. 2006, MNRAS, 365, 327
Heynderickx, D., Waelkens, C., & Smeyers, P. 1994, A&AS, 105, 447
Jerzykiewicz, M., Sterken, C., & Kubiak, M. 1988, A&AS, 72, 449
Kubiak, M., & Seggewiss, W. 1990, Acta Astron., 40, 85
Kuschnig, R., et al. 1997, A&A, 328, 544
Matthews, J. M., et al. 2004, Nature, 430, 51
Montgomery, M. H., & O'Donohue, D. 1999, Delta Scuti Newsletter, 13, 28
Morel, T., Butler, K., Briquet, M., Neiner, C., & Aerts, C. 2006, A&A, submitted
Niemczura, E., & Daszyńska-Daszkiewicz, J. 2005, A&A, 433, 659
Pamyatnykh, A. A., Handler, G., & Dziembowski, W. A. 2004, MNRAS, 350, 1022
Perryman, M. A. C., Lindegren, L., & Kovalevsky, J. 1997, A&A, 323, L49
Reegen, P., et al. 2006, MNRAS, in press
Scargle, J. D. 1982, ApJ, 263, 835
Stankov, A., & Handler, G. 2005, ApJS, 158, 193
Walker, G., et al. 2003, PASP, 115, 1023